J Membrane Biol (2015) 248:443–453
DOI 10.1007/s00232-014-9732-2

Dynamics of the Plasma Membrane Proton Pump

Federico Guerra · Ana-Nicoleta Bondar

Received: 15 June 2014 / Accepted: 18 September 2014 / Published online: 2 October 2014

Abstract Proton transfer over distances longer than that of a hydrogen bond often requires water molecules and protein motions. Following transfer of the proton from the donor to the acceptor, the change in the charge distribution may alter the dynamics of protein and water. To begin to understand how protonation dynamics couple to protein and water dynamics, here we explore how changes in the protonation state affect water and protein dynamics in the AHA2 proton pump. We find that the protonation state of the proton donor and acceptor groups largely affects the dynamics of internal waters and of specific hydrogen bonds, and the orientation of transmembrane helical segments that couple remote regions of the protein. The primary proton donor/acceptor group D684, can interact with water molecules from the cytoplasmic bulk and/or other protein groups.

Keywords Proton transfer · Protein dynamics · Dynamics of internal waters · Hydrogen-bonding · AHA2 proton pump

Introduction

Proteins such as the membrane-embedded proton pumps or the Photosystem II complex transport protons over long distances by using titratable protein sidechains and protein-bound water molecules as intermediate carriers for the proton. Flexibility of the protein and rearrangements of the water molecules may be required to establish paths for proton transfer. That protein and water dynamics are important for proton transfer is illustrated, for example, by observations on the bacteriorhodopsin proton pump: there, direct proton transfer from the primary donor to the proton acceptor has a rate-limiting barrier of $\sim$12 kcal/mol in a flexible protein environment, as compared to $\sim$23 kcal/mol when the protein is fixed (Bondar et al. 2006), the energetics of proton transfer is largely shaped by electrostatic interactions (Bondar et al. 2004; Braun-Sand et al. 2008), and active-site water molecules have a significant impact on the proton transfer path (Bondar et al. 2008). To probe the coupling between protonation state, protein and water dynamics, here we used as model system the P-type plasma membrane proton pump from *Arabidopsis thaliana*, AHA2 (Figs. 1a, 2a), for which we performed extensive all-atom molecular dynamics simulations with five different protonation states.

P-type ATPases are membrane proteins whose functioning involves hydrolysis of adenosine triphosphate (ATP) with formation of a phosphorylated (P) intermediate state. Proteins from this family, which includes cation pumps and phospholipid flipases (Kühlbrandt 2004; Morth et al. 2011; Palmgren and Nissen 2011), constitute important drug targets (Schubert and Peura 2008; Yatime et al. 2009). The plasma membrane proton pump couples the cleavage of ATP on the cytoplasmic side with protein conformational changes and proton transfer at the transmembrane domain, such that one proton is pumped across the membrane for each ATP molecule that is cleaved (for reviews see, for example, (Bublitz et al. 2010; Morth et al. 2011).

In the AHA2 plasma membrane proton pump, the primary proton donor is thought to be D684 of helix 6 (Pedersen et al. 2007; Buch-Pedersen et al. 2000; Buch-Pedersen and Palmgren 2003) (Figs. 1a, 2a). Mutation of

F. Guerra · A.-N. Bondar (✉)
Theoretical Molecular Biophysics, Department of Physics, Freie Universitaet Berlin, Arnimallee 14, 14195 Berlin, Germany
e-mail: nbondar@zedat.fu-berlin.de

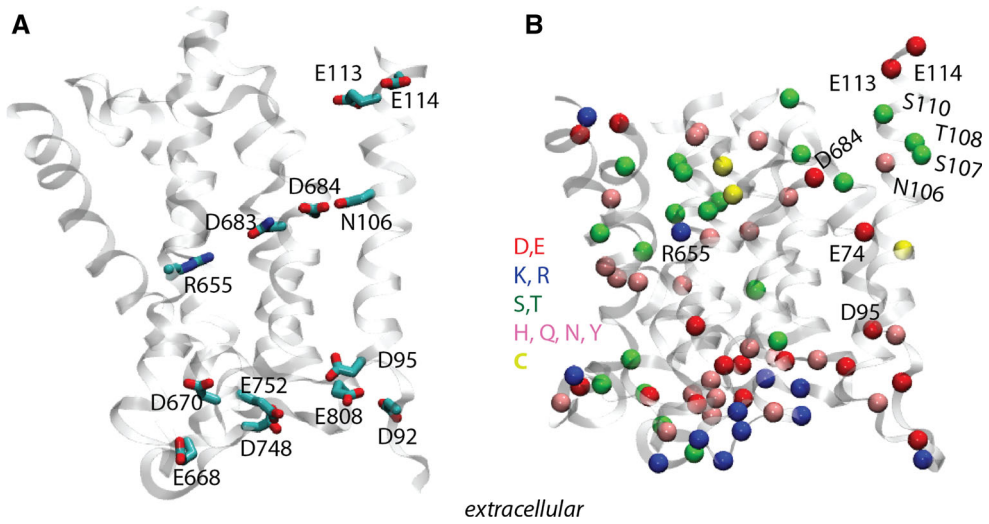

Fig. 1 Polar and charged groups of the transmembrane region of AHA2. **a** The transmembrane domain of AHA2 from the crystal structure of Pedersen et al. 2007 showing amino acid residues that may be particularly important for proton transfer. Oxygen atoms are *colored red*, nitrogen—*blue*, and carbon—*cyan*. **b** Charged and polar groups of the transmembrane domain of AHA2. For clarity, only the Cα atoms are depicted as *small spheres colored* as follows: Asp/Glu—*red*, Arg/Lys—*blue*, Ser/Thr—*green*, and other hydrogen bonding sidechains—*purple*. Cα atoms of Cys groups are shown in *dark yellow*. Note the numerous charged and polar groups in the both cytoplasmic and extracellular halves of the transmembrane domain. The primary proton donor/acceptor group, D684, is close to N106. Upstream N106 there are two carboxylates, E113 and E114, which in *N. crassa* and *S. cerevisiae* are present as Gln and Glu, respectively. For all molecular graphics we used VMD (Humphrey et al. 1996) (Color figure online)

D684 to asparagine, alanine, valine or arginine amino acid residues abolishes proton pumping (Buch-Pedersen and Palmgren 2003; Buch-Pedersen et al. 2000), and even the conservative D684E mutation reduces proton pumping to ~8 % of the wild-type level (Buch-Pedersen and Palmgren 2003). The observation of reduced proton pumping in D684E is somewhat counter-intuitive: a longer Glu sidechain, being more flexible, should allow the formation of a proton-transfer geometry with a lower energetic cost than an Asp sidechain (Bondar et al. 2006). The reduced pumping of D684E thus suggests that D684 has an important local interaction that is compromised when lengthening the carboxylate sidechain. This local interaction may be an inter-helical hydrogen bond with N106 on helix 2: in the crystal structure of AHA2 (Pedersen et al. 2007), the D684 carboxylate and the N106 carboxyamide group are within hydrogen bonding distance (Figs. 1a, 2a). The relevance of the N106/D684 interaction for the functional mechanism of the pump is further highlighted by the observations of perturbed proton pumping in N106 mutants (Ekberg et al. 2013).

The interaction between N106 and D684 may be dynamic: These two groups are close to an opening at the cytoplasmic side, where bulk water molecules are likely to visit transiently and interact favorably with, for example, E113/E114 (Fig. 1) (Buch-Pedersen et al. 2009). The presence of water molecules close to the proton-binding site was also inferred based on the 8 Å electron microscopy map of the *Neurosphora crassa* H^+-ATPase (Kühlbrandt et al. 2002). Upstream N106, helix 2 contains three Ser/Thr groups (S107, T108 and S110 in Fig. 1b); this NST*x*S motif is observed in some other plant H^+ P-type ATPases (Fagan and Saier 1994). On helix 6, 2–3 positions upstream the aspartate residue that acts as primary proton donor group, there is a Thr group—T686 in AHA2, and T733 in *N. crassa* and *S. cerevisiae*. These Ser/Thr groups may be important for the local dynamics and water interactions at the proton-binding site: the hydroxyl groups of Ser/Thr can have intrahelical hydrogen bonds (Gray and Matthews 1984; Presta and Rose 1988; Richardson and Richardson 1988) and alter the local dynamics of the helix (del Val et al. 2012).

We know little about the mechanism by which a proton released from D684 is translocated across the protein. Based on the crystal structure, it was suggested (Pedersen et al. 2007) that proton pumping may involve the D92/D95 carboxylate groups on the extracellular side (Fig. 1a). The distance between the putative proton donor and acceptor sites (17 Å between the Cγ atoms of D95 and D684 in Fig. 1a), is too large for a direct proton transfer, suggesting that proton transfer requires the assembly of a protein/water hydrogen bonded network. Although water coordinates have not been solved in the crystal structure, the significant number of polar groups within the transmembrane domain of the pump (Fig. 1b) suggests that numerous waters may visit the interhelical region of the protein at least transiently. Examples of groups that may be particularly important for water dynamics inside the

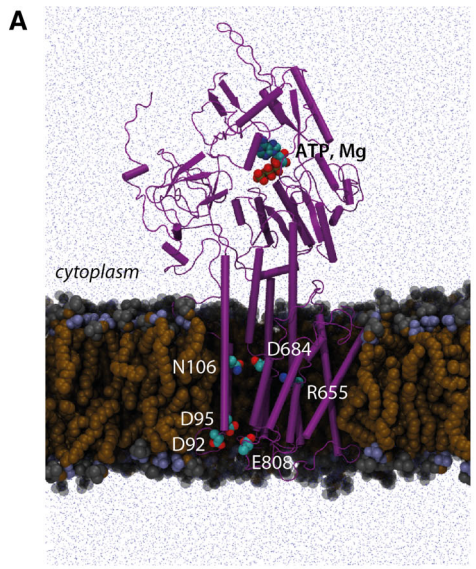

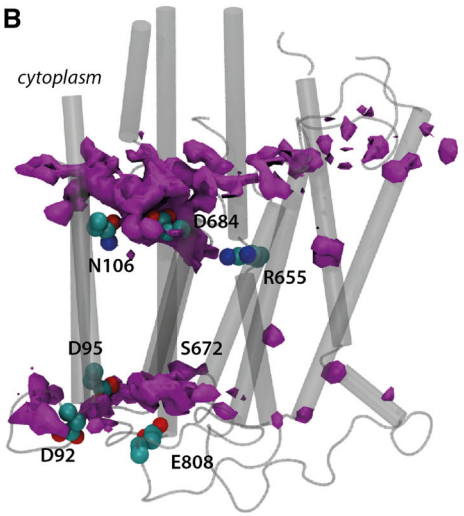

C

Simulation	Protein	Protonation	Length (ns)
Sim1	wild type	p-1	90
Sim2	wild type	p-2	100
Sim2′	R655A	p-2	100
Sim3	wild type	p-3	112
Sim4	wild type	p-4	115
Sim5	wild type	p-5	98
Sim5′	R655A	p-5	75

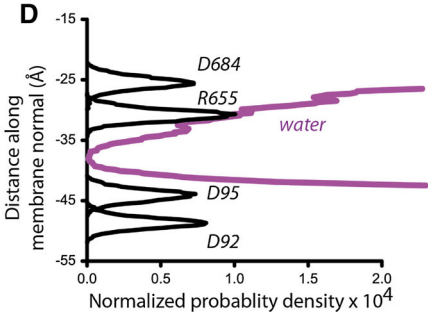

Fig. 2 AHA2 in a hydrated lipid membrane patch. **a** *Cut-away* view of the simulation system from the end of Sim1. The protein is depicted as magenta cartoons, water oxygen atoms as *blue dots*, and lipid molecules are shown as van der Waals spheres with the alkyl chains in ochre and the headgroups in *ice blue*. Important protein groups are depicted as van der Waals spheres using the *color* code from Fig. 1a. **b** *Close* view of the transmembrane region of AHA2 illustrating locations sampled by water molecules at the end of Sim1. The water locations are illustrated as an isosurface (isovalue 0.48) computed using 15 equally spaced coordinate snapshots from the last 6 ns of Sim1. **c** Summary of the simulations performed. For details on the protonation state, see Fig. 3. **d** Normalized probability distribution of water molecules and specific protein groups. For clarity, the water density profile is shown only for the transmembrane region of the protein (Color figure online)

transmembrane domain include E74, which is part of the first transmembrane helix, and R655, which is at the middle of helix 5 (Fig. 1). In the crystal structure (Pedersen et al. 2007), the positively charged sidechain of R655 is close to a cavity that might be filled with water (Buch-Pedersen et al. 2009). The suggestion that R655 likely interacts with water is compatible with the absence of nearby protein sidechains for hydrogen bonding. Instead, R655 is within hydrogen-bonding distance (3.4 Å) from the backbone carbonyl of S762.

To begin to understand the dynamics of AHA2 and how protein groups and waters respond to changes in its protonation state, we performed extensive all-atom molecular dynamics simulations of AHA2 for five different protonation states. We find that the transmembrane domain of AHA2 can host numerous water molecules. The protonation states of D95 and D684 appear important for inter-helical hydrogen bonding in the transmembrane region. The R655A mutant, which has drastically reduced proton pumping (Buch-Pedersen and Palmgren 2003), has altered water dynamics.

Methods

Protein Structure

For the starting protein coordinates we used chain A of the AHA2 crystal structure from Ref. (Pedersen et al. 2007) (PDB ID: 3B8C). This crystal structure indicates coordinates for a magnesium ion bound at the ATP site, and for a

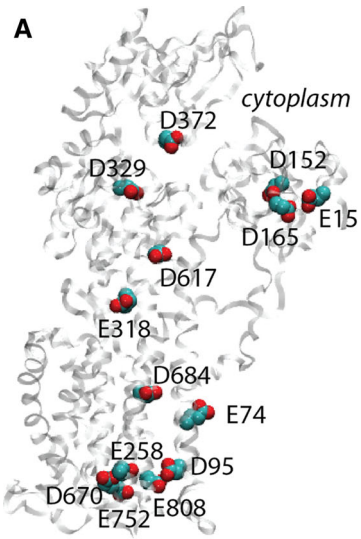

B

Protonation	Protonated Asp/Glu (*)
p-1	E15, D95, D165, D372
p-2	D684
p-3	E15, D165, D372, D684
p-4	E15, D165, D372
p-5	D95

Fig. 3 Protonation states studied with Sim1-Sim5. **a** Image based on the crystal structure of AHA2 (PDB ID:3B8C, chain A) (Pedersen et al. 2007) with carboxylate sidechains whose protonation state was considered here. **b** Carboxylate groups whose protonation distinguishes Sim1-Sim5. In all simulations performed, E74, D152, E258, E318, D329, D617, D670, E752 and E808 are protonated

nonhydrolysable ATP analogue, 5′-(β,γ-methylene)-triphosphate, AMPPCP. To model ATP, we replaced the C_3B carbon atom of AMPPCP by oxygen. We constructed coordinates for the hydrogen atoms using CHARMM (Brooks et al. 2009; Brooks et al. 1983), and used VMD (Humphrey et al. 1996) to align the protein with its principal axes along the *xyz* axes. We then embedded the protein into a palmitololeoyl phosphatidylcholine (POPC) lipid bilayer such that the protein was oriented with its principal axis along the membrane normal, and its transmembrane domain was in the center of the lipid bilayer. The lipid bilayer was solvated by 84,779 water molecules, and chloride ions were added for charge neutrality. The simulation system consisting of the protein, bound ATP and magnesium, hydrated lipid bilayer and neutralizing chloride ions, contained ~332,000 atoms.

To prepare the R655A mutant we used the crystal structure of wild-type AHA2 (Pedersen et al. 2007) and replaced the sidechain of R655 by Ala.

Protonation States

We explored the coupling of AHA2 dynamics to the protonation state by performing simulations with different protonation states of specific carboxylate groups. To select the protonation states we inspected the crystal structure and used PROPKA 3.1 (Li et al. 2005; Olsson et al. 2011; Sondergaard et al. 2011) to estimate the pKa values. This led us to select five different protonation states for further investigation with molecular dynamics simulations (Figs. 2c, 3). Except for the carboxylate groups explicitly listed as protonated in a specific simulation, all other titratable amino acid residues were considered in their standard protonation state.

Force Field Description

We used the CHARMM (Brooks et al. 2009; Brooks et al. 1983) force field parameters for the protein (MacKerell et al. 1998; MacKerell et al. 2004), lipid (Klauda et al. 2010) and nucleotide atoms (Foloppe and MacKerell 2000; MacKerell and Banavali 2000), and the TIP3P model for water molecules (Jorgensen et al. 1983).

Molecular Dynamics Simulations

All simulations reported here were performed independently using the following protocol. We performed all-atom molecular dynamics simulations with NAMD (Kale et al. 1999; Phillips et al. 2005). Bonds involving hydrogen atoms were constrained using SHAKE (Ryckaert et al. 1977). We used a switching function between 8 and 12 Å for the short-range real-space interactions, and the smooth particle mesh Ewald summation (Darden et al. 1993; Essmann et al. 1995) for the Coulomb interactions. To perform simulations in the *NPT* ensemble ($T = 300$ K, $P = 1$ barr) we used a Langevin dynamics scheme and a Nose–Hoover Langevin piston (Feller and MacKerell 1995; Martyna et al. 1994). To integrate the classical equations of motion we used an integration step of 1 fs during heating and the first ~1 ns of equilibration without constraints, after which we used the reversible multiple time-step algorithm (Grubmüller et al. 1991; Tuckermann and Berne 1992) with time-steps of 1 fs for the bonded forces, 2 fs for the short-range non-bonded, and 4 fs for the long-range electrostatic forces.

During minimization and the initial stage of equilibration we used weak harmonic constraints as follows. Heating and the first 1 ns equilibration were performed with weak harmonic constraints of 5 kcal/mol $Å^2$ on the protein,

ATP, and magnesium ion, and 2 kcal/mol Å^2 on all waters and on lipids further than 15 Å from the protein. We then released all constraints on the lipid atoms and performed an additional 1 ns of equilibration. In the next two steps, each involving 1 ns equilibration, we first lowered to 2 kcal/mol Å^2 the constraints on protein, magnesium, and ATP atoms, and then switched them off. Finally, the constraints on the water molecules were switched off and the simulation was continued without any constraints. In what follows, as origin of the simulation time we consider the moment when all constraints were switched off. For data analyses of the simulations we used VMD (Humphrey et al. 1996) and our own scripts. Normalized number density profiles were computed from the last ~20 to 22 ns of the simulations. As criterion for hydrogen bonding we used a distance between the donor/acceptor heavy atoms ≤3.5 Å. To compare the sequences of H^+ P-type ATPases from *A. thaliana*, *N. crassa* and *S. cerevisiae*, we used Clustal W (Larkin et al. 2007).

Results

We studied the dynamics of wild-type AHA2 on timescales of 90–112 ns by performing five independent molecular dynamics simulations distinguished by the protonation states of specific carboxylate groups (Figs. 2c, 3). Test estimations of p*K*a values with PROPKA 3.1 (Li et al. 2005; Olsson et al. 2011; Sondergaard et al. 2011) indicated that several Asp/Glu groups have pKa values ≥6.0; these groups are D95, D152, D165, E208, E258, D275, E318, D329, D372, D559, D617, D670, E708, E752, and E808 (Fig. 3a). For E15, E74 and D684 (Fig. 3a) the estimated pKa values were somewhat lower at 5.8, 5.9 and 5.8, respectively. Further inspection of the crystal structure (Pedersen et al. 2007) indicated that the protein interactions of some of these carboxylate sidechains are compatible with their being protonated: for example, the carboxylate groups of E318, D372, E752 and E808 are within hydrogen-bonding distances of other carboxylate groups, and the E74 carboxylate is within 2.8 Å distance of the S70 carbonyl group. D684 is close to N106, which led to the suggestion that these two groups may hydrogen bond and that the crystal structure may have captured AHA2 in an intermediate state with D684 is protonated (Pedersen et al. 2007).

Pursuant to the considerations above, as a first step towards understanding the proton-coupled dynamics of AHA2, in all simulations we considered that E74, D152, E258, E318, D329, D617, D670, E752 and E808 are protonated. The five simulations on wild-type AHA2 are then distinguished by the protonation states of E15, D95, D165, D372 and D684 (Fig. 3). The proton donor/acceptor group D684 is negatively charged in Sim1, Sim4 and Sim5, and neutral (protonated) in Sim2 and Sim3. D95 (Figs. 1a, 2a) is negatively charged in Sim2, Sim3 and Sim4, and neutral in Sim1 and Sim5. Sim1 and Sim4, which are distinguished

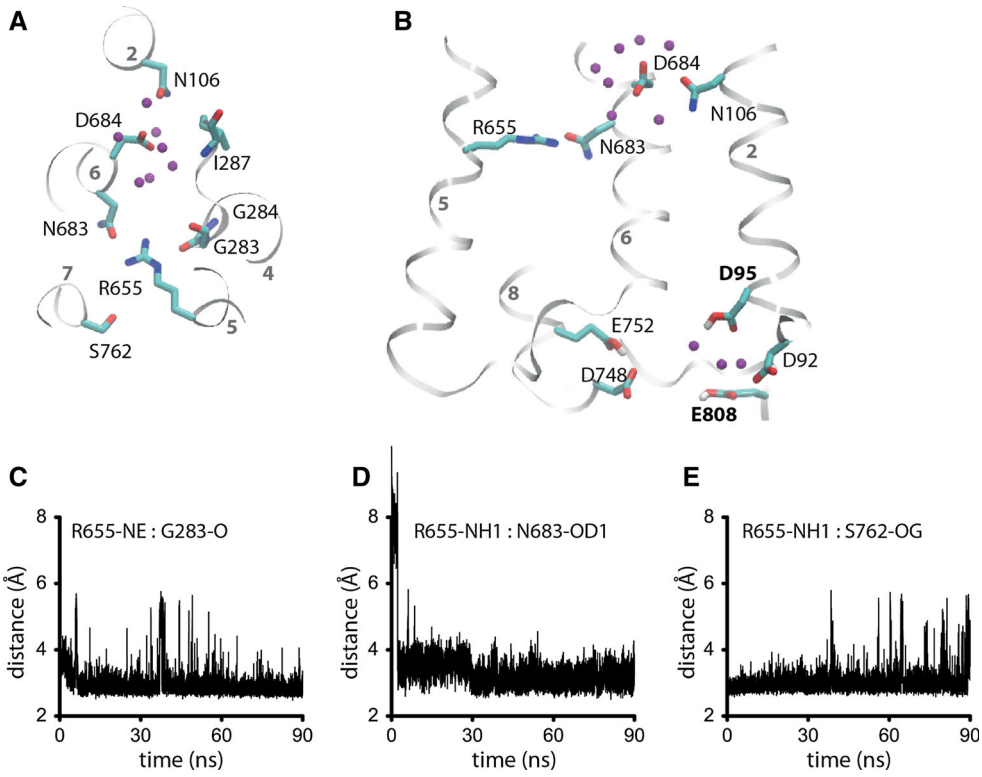

Fig. 4 Dynamics of AHA2 with negatively charged D684 and protonated D95 (Sim1). **a** *Close* view of interactions at the D684 site. Water molecules within 3.5 Å of D95 and D684 are depicted as *small purple* spheres. **b** Illustration of the interactions at the D95, R655 and D684 sites. **c**–**e** Time series of distances from Sim1 (in Å) indicating that R655 hydrogen bonds to G283 (**c**), N683 (**d**) and S762 (**e**). In Figs. 4b, 5a–c, 6d, and 9c, d, we label with *bold letters* the carboxylic amino acid residues that are protonated (Color figure online)

by the protonation state of D95, thus provide clues on how interactions at the extracellular proton release cluster may affect protein and water dynamics. Simulations on the R655A mutant (Sim2′ and Sim5′) were performed for the same protonation states as in the wild-type simulations Sim2 and Sim5 (Fig. 2c). We find that, regardless of the protonation state, there are numerous water molecules within the transmembrane domain of AHA2.

The Proton Donor Group D684 Interacts with Water Molecules

Due to its being located close to the cytoplasmic interface (Figs. 1a, 2a), D684 can easily interact with bulk water molecules regardless of its protonation state (Figs. 2b, 4a, b, 5a–c, 6a, b). At the extracellular side, the cluster of carboxylates (Fig. 1a) and other polar groups (Fig. 1b) is also accessible to water (Figs. 2a, b, 6a), and the normalized number density profiles (Figs. 2d, 6c) appear to suggest that water molecules can enter deeper into the extracellular region of the protein in Sim4, where D95 negatively charged, than in Sim1, where D95 is protonated. Accessibility of the pump to water from both sides of the membrane is also observed in Sim2, Sim3 and Sim5 (Fig. 5a, b). That a large number of water molecules can visit the transmembrane domain of the protein is compatible with the presence of numerous charged and polar protein groups in this region (Fig. 1).

Dynamics of the R655 Inter-helical Hydrogen Bonds

The location of R655 in the crystal structure and considerations of sequence/function relationship led to the suggestion that R655 may be important for its electrostatic interactions with D684, and for the generating a transmembrane potential (Pedersen et al. 2007). In computations with D684 negatively charged and D95 protonated (Sim1), we observe hydrogen bonding of R655 to N683 (Figs. 4b, c, d), the backbone carbonyl of G283 (Fig. 4c) and to the S762 hydroxyl group (Fig. 4e). That is, in Sim1 R655 can mediate a hydrogen-bonding cluster that interconnects helices 4, 5, 6 and 7 (Fig. 4a).

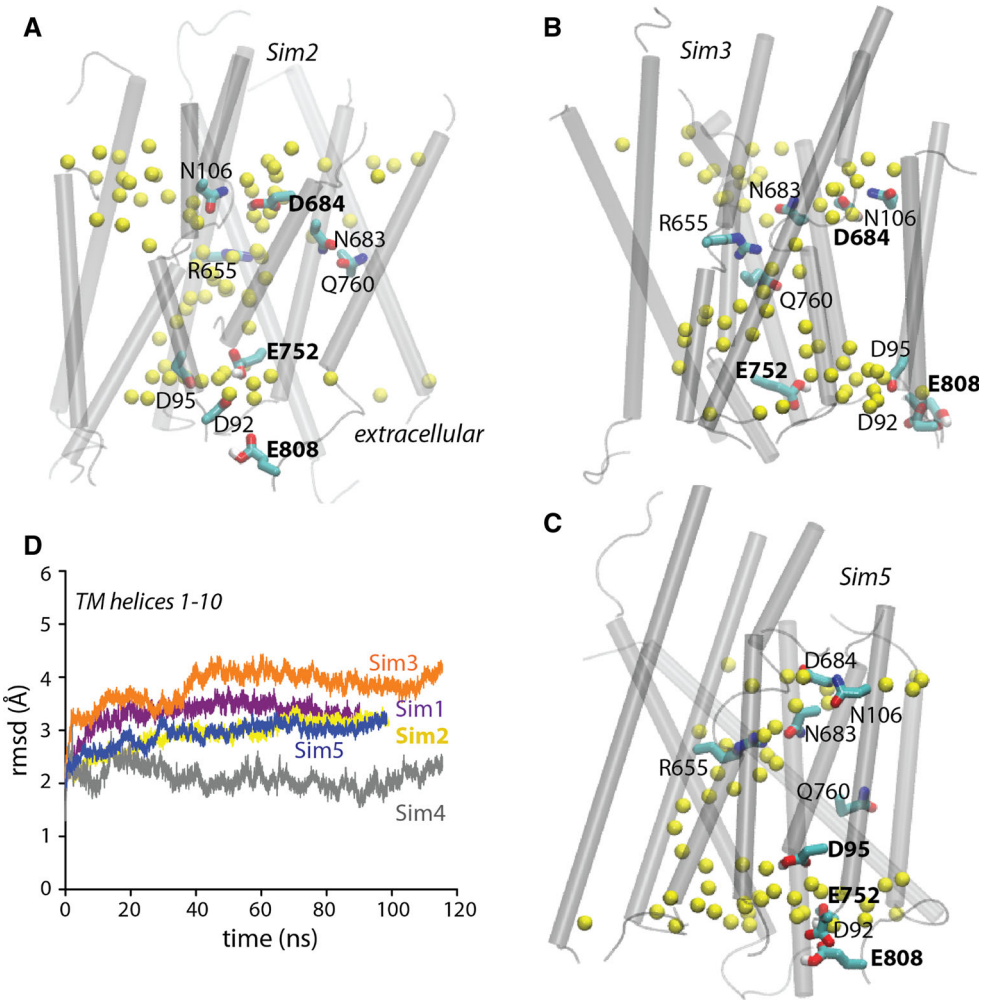

Fig. 5 Water molecules in the transmembrane domain of AHA2. **a–c** Snapshots from the end of Sim2 (**a**), Sim3 (**b**) and Sim5 (**c**) illustrating water molecules in the transmembrane domain of AHA2. Water oxygen atoms inside the inter–helical transmembrane region of the protein are shown as *yellow* spheres. For details on the protonation state of specific carboxylate groups in each of these three simulations, see Fig. 3. **d** Cα root-mean-squared distances (rmsd) relative to the starting crystal structure coordinates for the 10 transmembrane helices of AHA2 (Color figure online)

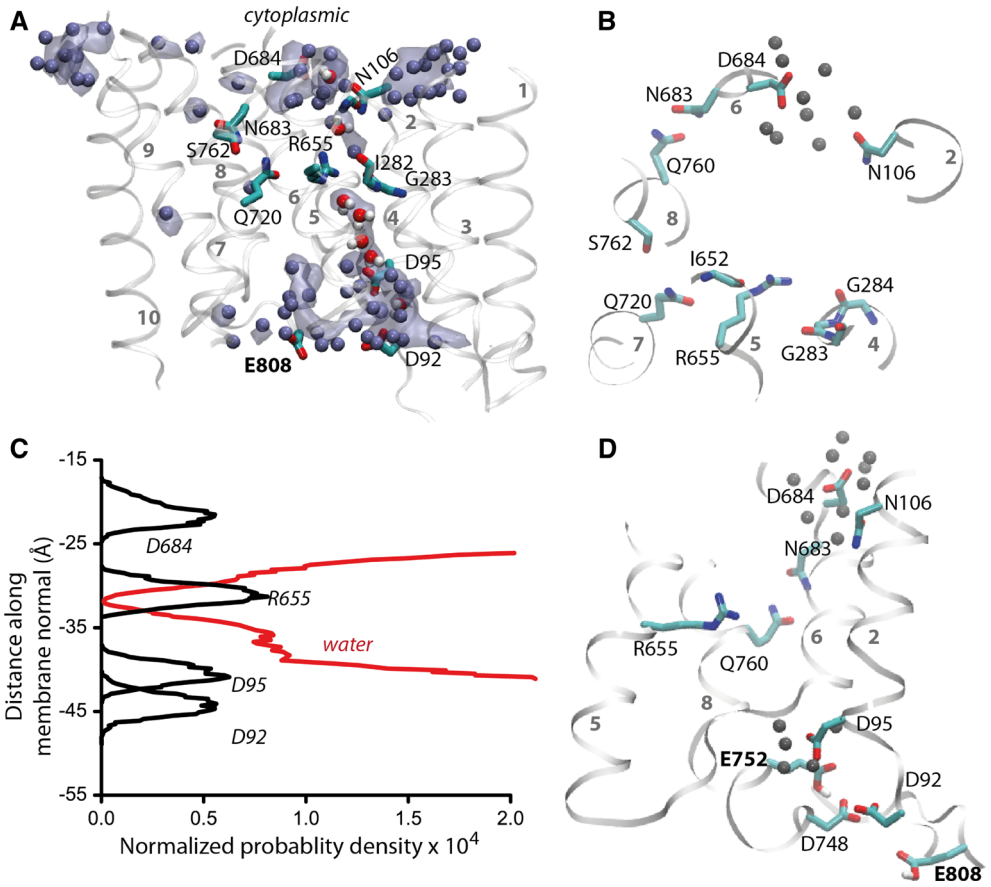

Fig. 6 Dynamics of AHA2 with negatively-charged D95 and D684. **a** Illustration of water molecules inside the transmembrane region of the protein in Sim4. The *ice-blue* surface is the isodensity surface of internal water molecules computed with VMD (Humphrey et al. 1996) from the last 20 ns of Sim4, shown at an isovalue of 0.4. The water isodensity surface is shown on a coordinate snapshot of the protein. For this coordinate snapshot we also depict as *spheres* (*red* for oxygen atoms and *white* for hydrogen) the water molecules along the pore from D684 to R655, and from R655 to D92/D95, that are within hydrogen-bonding distance from each other. **b** Interactions at the R655 and D684 sites. We show as *small gray spheres* the water oxygen atoms within 3.5 Å of the D684 carboxylate oxygen atoms and the N106 carboxyamide oxygen and nitrogen atoms. **c** Normalized density profiles for water and specific groups computed from Sim4. **d** Illustration of specific inter–helical interactions at the end of Sim4. We show as *small gray spheres* the water oxygen atoms from **b**, and those within 3.5 Å from the carboxyl oxygen atoms of E752 (Color figure online)

The inter-helical hydrogen-bonding cluster appears perturbed in Sim4, where the hydrogen bond between R655 and N683 breaks (Figs. 6a, b, d, 7). R655 now has a stable intra-helical hydrogen bond with the I652 backbone carbonyl group (Fig. 7e), and transient hydrogen bonds to the backbone carbonyls of G283 and G284 (Fig. 7c, d), whereas N683 engages in two stable hydrogen bonds with Q760 (Figs. 6b, 7a, b)—an amino acid residue that is only two helical turns upstream E752 (Fig. 6d). The changes in the inter-helical hydrogen bonds and water interactions at the N683, R655 and D95 sites appear associated with changes in the orientation of helices 2 and 5 relative to the membrane normal (Fig. 8a), such that the projection on the membrane plane of Ca atoms at the cytoplasmic interface of these helices changes by a few Å (Fig. 8b).

The observation above that the R655 sidechain may have transient hydrogen bonds to the backbone carbonyls of G283 and G284 is intriguing: It has been inferred, based on homology modeling, that the backbone carbonyls of I282, G283 and I285 could contribute to a binding site for a protonated water molecule (Bukrinsky et al. 2001), and found that replacement of I282 by Ala, Gly or Ser affects proton transfer (Fraysse et al. 2005). Hydrogen bonding of an Arg sidechain to backbone carbonyl groups could also indicate a structural role of the Arg (Borders et al. 1994).

The R655A Mutation Affects Water and Hydrogen Bond Dynamics

We tested the structural role of R655 by performing two independent simulations on the R655A mutant with D95

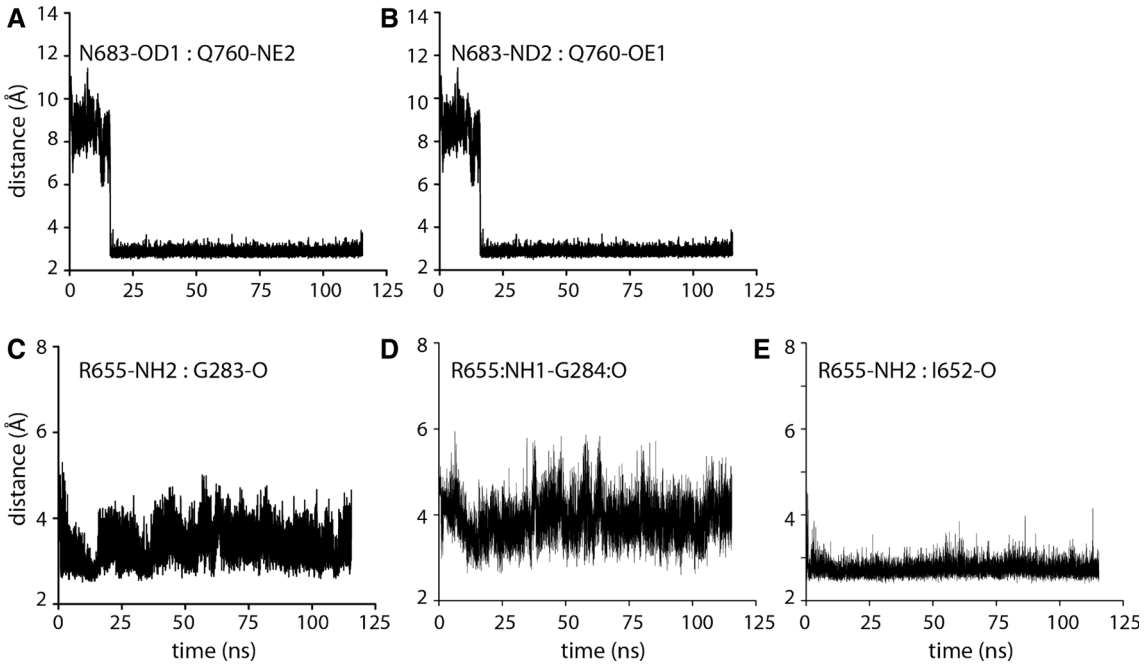

Fig. 7 Hydrogen bonding of R655 and N683 in Sim4. **a**–**e** Time series of selected distances from Sim4. N683 hydrogen bonds to Q670 (**a**, **b**), and R655 has transient inter-helical hydrogen bonds with the backbone carbonyl groups of G283 and G284 (**c**, **d**), and a stable intra-helical hydrogen bond with the I652 carbonyl group (**e**)

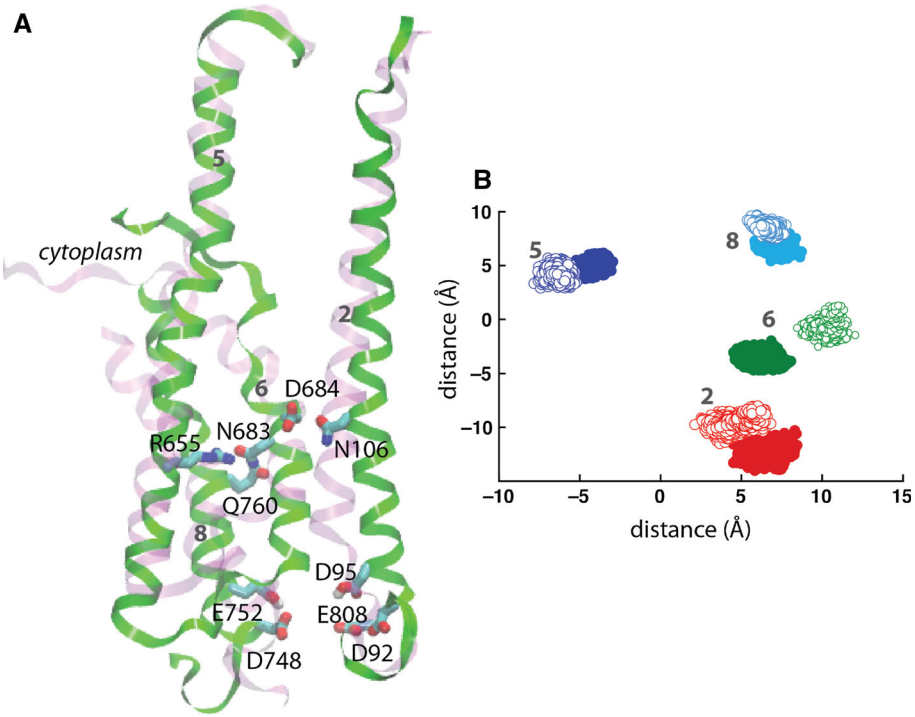

Fig. 8 The protonation state can affect the dynamics of the transmembrane domain of AHA2. **a** Overlap between protein structures from the end of Sim1 (*green*) and Sim4 (*transparent purple*). Selected amino acid sidechains are depicted as bonds using the geometry from Sim1. **b** Projection on the membrane plane of the Cα coordinates of amino acid residues from the cytoplasmic region of selected helices. The analysis was done by performing rms fits of the coordinate snapshots from the last 20 ns of Sim1 and Sim4 onto the starting protein coordinates (Color figure online)

negatively charged and D684 protonated (Sim2′), vs. D95 protonated and D684 negatively charged (Sim5′). Comparison of inter-helical hydrogen bond dynamics in the wild type versus R655A highlights the importance of the R655 sidechain for inter-helical interactions within the transmembrane domain (Fig. 9). In the wild type (Sim2) the protonated E74 carboxylate hydrogen bonds to the backbone carbonyl group of I99 on helix 2 (Fig. 9a). Helix 2 can further bridge to helix 6 via a transient hydrogen bond between N106 and D684 (Fig. 9c), and D684

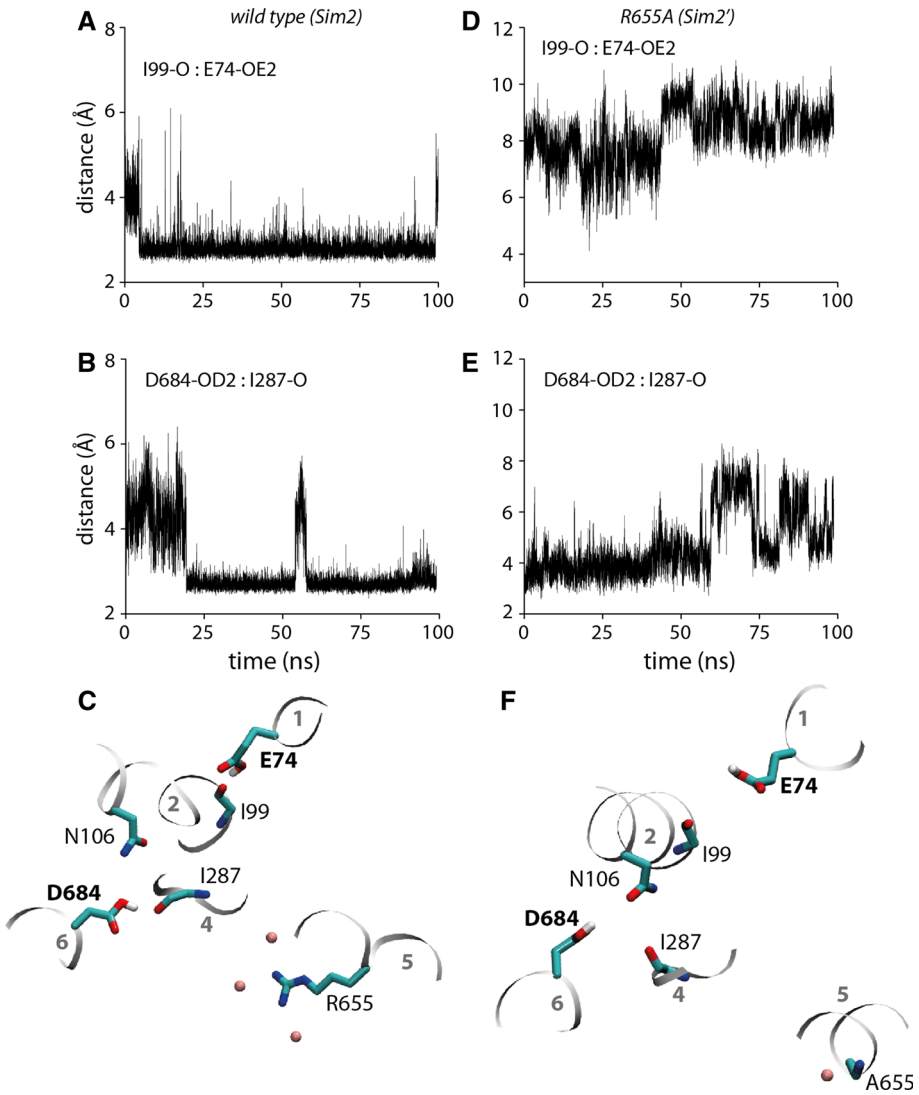

Fig. 9 Selected interactions in the wild-type protein and the R655A mutant with negatively-charged D95 and protonated D684. **a** and **b** Time series of selected distances (in Å) from Sim2. **c** Coordinate snapshot illustrating specific interactions at the end of Sim2. In addition to the hydrogen bond to the I287 carbonyl group, in Sim2 the protonated D684 carboxyl group has transient hydrogen bonding with the N106 carboxyamide group. **d**, **e** Time series of corresponding interactions in the R655A mutant (Sim2′). Note that in the mutant the inter-helical interactions of E74 and D684 are perturbed. **f** Snapshot from the end of Sim2′ illustrating specific interactions in a simulation of the R655A mutant with the same protonation states as in Sim2. The hydrogen bond between E74 and the backbone carbonyl of I99 is also absent in Sim5′

connects to the backbone carbonyl of I287 (Fig. 9b). These inter-helical hydrogen bonds appear perturbed in the R655A mutant (Sim2′, Fig. 9d–f).

Conclusions

We performed all-atom simulations on wild type AHA2 plasma membrane proton pump with different protonation states of specific carboxlate groups. The simulations suggest tight coupling between the protonation state, protein and water dynamics. Such a tight coupling may be necessary to coordinate the ATP hydrolysis steps and protein translocation during the reaction cycle of the pump.

The inter-helical domain of the pump is accessible to water from both sides of the membrane (see examples in Figs. 5a–c), and there is water close to D684 in all simulations of the wild-type pump (Figs. 2a, 5a–c, 6a). Though the presence of numerous water molecules inside the transmembrane domain of the pump is compatible with the presence of numerous charged and polar amino acid residues at the both cytoplasmic and extracellular sides of the transmembrane region of the protein (Fig. 1b), the accessibility to water from both sides of the membrane may be detrimental to directional proton pumping if accompanied by uncoordinated formation of proton-transfer wires. Based on considerations of water accessibility, the observation of an apparently smaller accessibility to water of AHA2 in Sim1 (Fig. 2d) as compared to Sim2-Sim5 (Figs. 5a–c, 6a–c) could be interpreted to suggest that in the crystal structure D684 might be unprotonated, whereas D95 is neutral. We think, however, that a conclusion on the protonation states of specific carboxylate groups would be premature. All-atom molecular dynamics simulation on several different membrane transporters demonstrated the transient sampling of states that allow the passage of water

molecules, leading to the proposal that such water-conducting states might represent a general feature of membrane transporters (Li et al. 2013). In the case of our AHA2 simulations, we think that the sensitivity of the protein dynamics to the protonation state of specific carboxylates highlights the need of a systematic assessment of the dynamics for other possible protonation states of the pump that were not considered here. For example, during simulations we observe that some of the carboxylates for which PROPKA3.1 indicated elevated pKa values (e.g., E15, E808) face the bulk water, suggesting that they may be unprotonated. Further assessment of the protonation-coupled protein and water dynamics would benefit greatly from a high resolution crystal structure: The moderate resolution of the crystal structure of AHA2, 3.6 Å (Pedersen et al. 2007) may be insufficient to accurately resolve details of inter-helical hydrogen bonds, which could potentially affect the computation of protonation states and the dynamics of the protein and water molecules.

Hydrogen bonds are important determinants of the structure and dynamics of a membrane protein (see, for example, (Bondar and White 2012; Cao and Bowie 2012; White and Wimley 1999). The transmembrane domain of the protein is rich in charged and polar groups that can hydrogen bond (Fig. 1). There are several Ser/Thr groups close to important sites of the protein (Fig. 1)—for example, S107, T108 and S110 upstream N106 on helix 2; S651 and T653 downstream R655 on helix 5; T686 and T689 upstream D684; S762 and S765 upstream Q760 on helix 8. The presence of these hydroxyl groups is intriguing, because simulations on model transmembrane helices and on bacteriorhodopsin suggest that Ser/Thr groups can influence the local dynamics of the helices and their water interactions (del Val et al. 2014, 2012). In the yeast PMA1 H^+ ATPase, the S699A and S699C mutations (corresponding to AHA2 T653) drastically impair proton pumping (Morsomme et al. 2000).

The dynamics of inter-helical hydrogen bonds involving carboxylic amino acid residues can depend significantly on whether or not the carboxylate is protonated. Differences in the dynamics of inter-helical hydrogen bonds can in turn affect the local water interactions and the relative orientation of the helices, which can help relay conformational changes to remote distances in the protein. This highlights the need of accurate information on the identity of protonated carboxylate sidechains along the proton-pumping reaction cycle of AHA2. An important open question is whether proton transfer starts from a conformer in which there are at least two protons bound to the transmembrane region, at the cytoplasmic (D684) and extracellular carboxylate clusters.

Acknowledgments This work was supported in part by the Marie Curie International Reintegration Award FP7-PEOPLE-2010-RG 276920 (to A-NB) and by an allocation of computing time from the North-German Supercomputing Alliance (HLRN bec00076). FG was supported in part by the DFG Collaborative Research Center SFB 1078 'Protonation dynamics in protein function', Project C4 (to A-NB).

References

Bondar A-N, White SH (2012) Hydrogen bond dynamics in membrane protein function. Biochim Biophys Acta 2012:942–950

Bondar A-N, Fischer S, Smith JC, Elstner M, Suhai S (2004) Key role of electrostatic interactions in bacteriorhodopsin proton transfer. J Am Chem Soc 126:14668–14677

Bondar A-N, Smith JC, Fischer S (2006) Structural and energetic determinants of primary proton transfer in bacteriorhodopsin. Photochem Photobiol Sci 5:547–552

Bondar A-N, Baudry J, Suhai S, Fischer S, Smith JC (2008) Key role of active-site water molecules in bacteriorhodopsin proton-transfer reactions. J Phys Chem B 112:14729–14741

Borders CLJ, Broadwater JA, Bekeny PA, Salmon JE, Lee AS, Eldridge AM, Pett VB (1994) A structural role for arginine in proteins: Multiple hydrogen bonds to backbone carbonyl oxygens. Prot Sci 3:541–548

Braun-Sand S, Sharma PK, Chu ZT, Pisliakov AV, Warshel A (2008) The energetics of the primary proton transfer in bacteriorhodopsin revisited: it is a sequential light-induced charge separation after all. Biochim Biophys Acta 1777:441–452

Brooks BR et al (2009) CHARMM: the biomolecular simulation program. J Comput Chem 30:1545–1614

Brooks BR, Bruccoleri RE, Olafson BD, States DJ, Swaminathan S, Karplus M (1983) CHARMM: a program for macromolecular energy, minimization, and dynamics. J Comput Chem 4:187–217

Bublitz M, Poulsen H, Morth JP, Nissen P (2010) In and out of the cation pumps: P-type ATPase structure revisited. Curr Opin Struct Biol 20:431–439

Buch-Pedersen MJ, Palmgren MG (2003) Conserved Asp684 in tramsmebrane segment M6 of the plant plasma membrane P-type proton pump AHA2 is a molecular determinant of proton translocation. J Biol Chem 278:17845–17851

Buch-Pedersen MJ, Venema K, Serrano R, Palmgren MG (2000) Abolishment of proton pumping and and accumulation in the E_1P conformational state of a plant plasma membrane H^+ATPase by substitution of a conserved aspartyl residue in transmembrane segment 6. J Biol Chem 275:39167–39173

Buch-Pedersen MJ, Pedersen BP, Veierskov B, Nissen P, Palmgren MG (2009) Protons and how they are transported by proton pumps. Pflug Arch-Eur J Physiol 457:573–579

Bukrinsky JT, Buch-Pedersen MJ, Larsen S, Palmgren MG (2001) A putative binding site of plasma membrane H^+ -ATPase identified through homology modeling. FEBS Lett 494:6–10

Cao Z, Bowie JU (2012) Shifting hydrogen bonds may produce flexible transmembrane helices. Proc Natl Acad Sci USA 109:8121–8126

Darden T, York D, Pedersen L (1993) Particle mesh Ewald: an N × log(N) method for Ewald sums in large systems. J Chem Phys 98:10089–10092

del Val C, White SH, Bondar A-N (2012) Ser/Thr motifs in transmembrane proteins: conservation patterns and effects on local protein structure and dynamics. J Membr Biol 245:717–730

del Val C, Bondar L, Bondar A-N (2014) Coupling between inter-helical hydrogen bonding and water dynamics in a proton transporter. J Struct Biol 2014(186):95–111

Ekberg K, Wielandt AG, Buch-Pedersen MJ, Palmgren MG (2013) A conserved asparagine in a P-type proton pump is required for efficient gating of protons. J Biol Chem 288:9610–9618

Essmann U, Perera L, Berkowitz ML, Darden T, Lee H, Pedersen LG (1995) A smooth particle mesh Ewald method. J Chem Phys 103:8577–8593

Fagan MJ, Saier MH Jr (1994) P-type ATPases of eukaryotes and bacteria: sequence analysis and construction of phylogenetic trees. J Mol Evol 38:57–99

Feller SE, MacKerell AD Jr (1995) Constant pressure molecular dynamics simulation: the Langevin piston method. J Chem Phys 103:4613–4621

Foloppe N, MacKerell AD Jr (2000) All-atom empirical force field for nucleic acids: 1) Parameter optimization based on small molecule and consdensed phase macromolecular target data. J Comput Chem 21:86–104

Fraysse ÅS, Møller ALB, Poulsen LR, Wollenweber B, Buch-Pedersen MJ, Palmgren MG (2005) A systematic mutagenesis study of Ile-282 in transmembrane segment M4 of the plasma membrane H^+-ATPase J Biol Chem 280:21785-21790

Gray TM, Matthews BW (1984) Intrahelical hydrogen bonding of serine, threonine and cysteine residues within a-helices and its relevance to membrane-bound proteins. J Mol Biol 175:75–81

Grubmüller H, Heller H, Windermuth A, Schulten K (1991) Generalized Verlet algorithm for efficient molecular dynamics simulations with long-range interactions. Mol Simul 6:121–142

Humphrey W, Dalke W, Schulten K (1996) VMD: visual molecular dynamics. J Mol Graph 14:33–38

Jorgensen WL, Chandrasekhar J, Madura JD, Impey RW, Klein ML (1983) Comparison of simple potential functions for simulating liquid water. J Chem Phys 79:926–935

Kale L et al (1999) NAMD2: greater scalability for parallel molecular dynamics. J Comput Chem 151:283–312

Klauda JB et al (2010) Update of the CHARMM all-atom additive force field for lipids: validation on six lipid types. J Phys Chem B 114:7830–7843

Kühlbrandt W (2004) Biology, structure and mechanism of P-type ATPases. Nature Rev Mol Cell Biol 5:282–295

Kühlbrandt W, Zeelen J, Dietrich J (2002) Structure, mechanism and regulation of the *Neurospora* plasma membrane H^+ -ATPase. Science 297:1692–1696

Larkin MA et al (2007) Clustal W and Clustal X version 2.0. Bioinformatics 23:2947–2948

Li H, Robertson AD, Jensen JH (2005) Very fast empirical prediction and interpretation of protein pKa values. Proteins 61:704–721

Li J, Shaikh SA, Enkavi G, Wen P-C, Huang Z, Tajkhorshid E (2013) Transient formation of water-conducting states in membrane transporters. Proc Natl Acad Sci USA 110:7696–7701

MacKerell AD Jr, Banavali N (2000) All-atom empirical force field for nucleic acids: 2) Application to molecular dynamics simulations of DNA and RNA in solution. J Comput Chem 21:105–120

MacKerell AD Jr, Feig M (2004) Brooks CL III Extending the treatment of backbone energetics in protein force fields: limitations of gas-phase quantum mechanics in reproducing protein conformational distributions in molecular dynamics simulations. J Comput Chem 25:1400–1415

MacKerell AD Jr et al (1998) All-atom empirical potential for molecular modeling and dynamics studies of proteins. J Phys Chem B 102:3586–3616

Martyna GJ, Tobias DJ, Klein ML (1994) Constant-pressure molecular-dynamics algorithms. J Chem Phys 101:4177–4189

Morsomme P, Slayman CW, Goffeau A (2000) Mutagenic study of the structure, function and biogenesis of the yeast plasma membrane H^+-ATPase. Biochim Biophys Acta 1469:133–157

Morth JP, Pedersen BP, Buch-Pedersen MJ, Andersen JP, Vilsen B, Palmgren MG, Nissen P (2011) A structural overview of the plasma membrane Na^+, K^+-ATP-ase and H^+-ATPase ion pumps. Nat Rev Mol Cell Biol 12:60–70

Olsson MHM, Sondergaard CR, Rostowski M, Jensen JH (2011) PROPKA3: consistent treatment of internal and surface residues in empirical pKa predictions. J Chem Theory Comput 7:525–537

Palmgren MG, Nissen P (2011) P-type ATPases. Annu Rev Biophys 40:243–266

Pedersen BP, Buch-Pedersen MJ, Morth JB, Palmgren MG, Nissen P (2007) Crystal structure of the plasma membrane proton pump. Nature 450:1111–1114

Phillips JC et al (2005) Scalable molecular dynamics with NAMD. J Comput Chem 26:1781–1802

Presta LG, Rose GD (1988) Helix signals in proteins. Science 240:1632–1641

Richardson JS, Richardson DC (1988) Amino acid preferences for specific locations at the end of helices. Science 240:1648–1652

Ryckaert J-P, Ciccotti G, Berendsen HJC (1977) Numerical integration of the Cartesian equations of motion of a system with constraints Molecular dynamics of n-alkanes. J Comput Phys 23:327–341

Schubert ML, Peura DA (2008) Control of gastric acid secretion in health and disease. Rev Basic Clin Gastroeneterol 134:1842–1860

Sondergaard CR, Olsson MHM, Rostowski M, Jensen JH (2011) Improved treatment of ligands and coupling effects in empirical calculation and rationalization of pKa values. J Chem Theor Comput 7:2284–2295

Tuckermann M, Berne BJ (1992) Reversible multiple time scale molecular dynamics. J Chem Phys 97:1990–2001

White SH, Wimley WC (1999) Membrane protein folding and stability: physical principles. Annu Rev Biomol Struct 28:319–365

Yatime L et al (2009) P-type ATPases as drug targets: tools for medicine and science. Biochim Biophys Acta 1787:207–220